AIChE

Surfactant-Free Microdispersion Process of Gas in Organic Solvents in Microfluidic Devices

J. Tan, L. Du, J. H. Xu, K. Wang, and G. S. Luo
The State Key Lab of Chemical Engineering, Dept. of Chemical Engineering, Tsinghua University, Beijing 100084, China

DOI 10.1002/aic.12487
Published online December 29, 2010 in Wiley Online Library (wileyonlinelibrary.com).

The scaling of bubble/slug formation in organic solvents at microscale without surfactant was initially investigated by using T-junction and symmetrically cross-shaped microfluidic devices. Four unique organic solvents and three dispersion methods were used, forming different flow patterns and dispersion size. The flow pattern of uniform slug flow was investigated. Both the gas–liquid flow and dispersion size, which ranged from 400 to 1400 μm in length and 270 to 430 μm in diameter, depended on several factors including dispersion method, two-phase flow rates, physical properties of the liquid phase, and structure of microchannels. A general equation $L/w = k(Q_G/Q_L)^{\alpha}Ca^{\beta}$ *was used to characterize the dispersion size with modification of* Q_G/Q_L *for different dispersion methods, considering the influences of breakup rate and transformation of the interface shape on the dispersion process. Three models were developed to predict the dispersion size for different dispersion methods, and calculated data were in good agreement with the experimental results.* © 2010 American Institute of Chemical Engineers
AIChE J, 57: 2647–2656, 2011
Keywords: microfluidic, gas–liquid, organic solvents, scaling

Introduction

In the recent years, microbubbles have caught the attention of many researchers for their numerous and diverse applications, such as ultrasound contrast agents, therapies for thrombus destruction, and new targeted drug delivery and flotation column methods.[1–4] Particularly, in the chemical industry, gas–liquid microdispersed systems can provide large interfacial areas, fast mixing, and reduced heat/mass transfer limitations, compared with the conventional bench-scale systems. As a result, gas–liquid microdispersed systems have recently been used for mass transfer operations and reactions process, taking gas absorption/desorption,[5] halogenations,[6–9] nitrations,[10] and hydrogen peroxide synthesis[11] as examples. Segmented bubbles can also be used as one of the methods to induce a recirculatory flow to enhance the mixing.[12–14] In all of the applications mentioned above, the bubble size and distribution are key parameters.

In the last 2 decades, microfluidic devices have shown their potential applications in on-chip separations,[15–17] kinetic analysis,[18,19] and protein crystallization.[20,21] Currently, several techniques exist for the generation of bubbles, and the formation mechanism is discussed. Ganan-Calvo et al. described the formation of monodisperse gas bubbles using a hydrodynamic flow focusing method through capillaries[22,23] and orifices.[24] They found that bubble was formed for the absolute instabilities of the gas phase when surrounded by liquid stream.[23] Garstecki et al. produced monodisperse bubbles by using a flow focusing devices and found that the continuous fluid rate entirely control the breakup dynamics

Correspondence concerning this article should be addressed to G. S. Luo at gsluo@tsinghua.edu.cn.

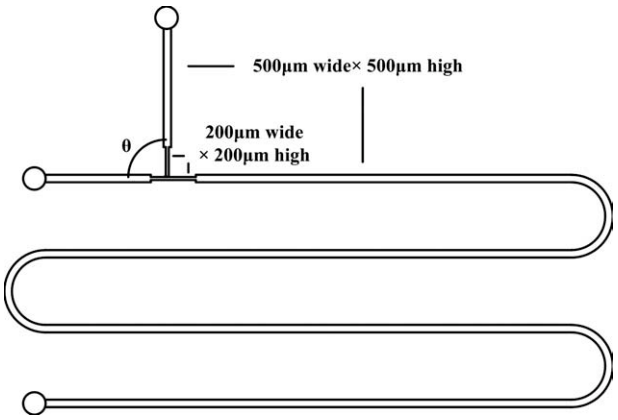

Figure 1. T-junction microfluidic device with intersection angle θ.

($\theta = 30°$, 60°, 90°, 120°, and 150°).

and the volume of the bubbles, V_b, scaled with the flow rate of the gas stream, Q_G, and the flow rate of the liquid stream, Q_L, according to $V_b \propto Q_G/Q_L$.[25,26] Yasuno et al. prepared monodisperse microbubbles on a microchannel plate with a geometry-dominated breakup method on and found that the parameters mainly affecting the bubble/slug size contained the operating conditions and the physical properties including surface/interfacial tension and continuous-phase viscosity.[27] Xu et al. described the formation of monodisperse microbubbles in a T-junction microfluidic device using a cross-flow rupturing technique.[28] Their study showed that the bubble size, d_b, can be controlled as $d_b \propto 1/u_L\mu_L$, in which u_L was the liquid flow rate and μ_L was the liquid viscosity. In our previous work, monodisperse microbubbles were prepared using a perpendicular rupturing flow route in a T-junction microfluidic device. The formation process was considered to be affected by the balance between shear force of the continuous flow and interfacial tension and the deformation of the two-phase interface.[29]

As mentioned above, a lot of work has been carried out to study the mechanism of gas–liquid dispersion process in microfluidic devices. The vast majority of these efforts are focused on the process of gas dispersed in water/aqueous solutions with addition of surfactant. Few studies on gas microdispersion in organic solvents have been performed, especially for working systems without surfactant. However, the systems of gas dispersed in organic solvents have important applications in many gas–liquid reaction and separation processes, such as absorption, halogenations,[6–9] nitrations,[10] and gas–liquid catalytic hydrogenation.[30] A systematical study on the surfactant-free microdispersion of gas in organic solvents could be very useful for realizing the intensification of gas/liquid separation and chemical reaction processes in microdevices. In this article, the scaling of bubble/slug formation in organic solvents at microscale is initially investigated by using T-junction and symmetrically cross-shaped microfluidic devices. The two types of channel geometries and three dispersion methods are simple and typical method to achieve microdispersion by direct contact of two phases and, thus, suitable to understand the basic law of microdispersion processes. The microdispersed systems of gas in several different organic solvents without surfactant are produced. Different flow patterns as the variation of the physical properties of the liquid phases and operation conditions are demonstrated. The influences of the dispersion method, geometric structures, physical properties of the liquid phases, and operation conditions on dispersion size are investigated. Furthermore, the mechanisms of the formation of microbubbles in organic solvents are discussed, and a quantitative correlation is developed to predict the microbubbles size.

Experimental

Microfluidic device

Three groups of microfluidic devices were used in the experiments, respectively. Each microfluidic device was fabricated on a 60 mm × 40 mm × 2 mm polymethyl methacrylate (PMMA) plate using an end mill and sealed using another 60 mm × 40 mm × 2 mm PMMA plate with ultrasonic-assisted sealing technique.[31]

Group (A) and Group (B) are exactly the same, containing five T-junction microfluidic devices with differing angles of intersection, respectively. For each device in this group, both the straight and intersecting channels are 500 μm wide × 500 μm high. At the intersection, both channels become narrower, 200 μm wide × 200 μm high, with the narrow section on the intersecting channel 1 mm in length and the narrow section on the straight channel 3 mm in length (1 mm before intersection and 2 mm after intersection; Figure 1).

Group (C) consists of four symmetrically cross-shaped microfluidic devices with differing angles of intersection. The size is similar to the T-junction microfluidic devices above. For each device in this group, the two intersecting channels and the straight channel are 500 μm wide × 500 μm high. At the intersection, both channels become narrower, 200 μm wide × 200 μm high, with the narrow section on the intersecting channel 1 mm in length and the narrow section on the straight channel 3 mm in length (1 mm before intersection and 2 mm after intersection; Figure 2).

Two microsyringe pumps were used to pump the two phases into the two flow channels. For Group (A) of T-junction microfluidic devices, the liquid phase was pumped into the

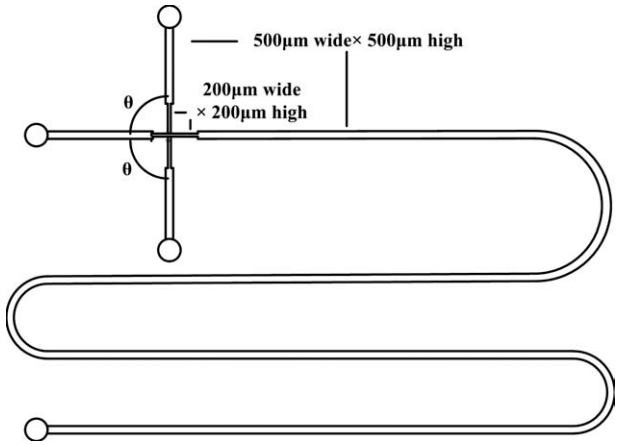

Figure 2. Symmetrically cross-shaped microfluidic device with intersection angle θ.

($\theta = 30°$, 60°, 90°, and 120°).

Table 1. Physical Properties of the Organic Working Systems (25°C)

	Composition	Density (g/cm^3)	Viscosity (mPa s)	Surface Tension (mN/m)
System 1	Dodecane	0.7455	1.38	22.66
System 2	67 wt % Dodecane, 33 wt % hexadecane	0.7527	1.77	23.06
System 3	Hexadecane	0.7714	3.03	23.64
System 4	67 wt % hexadecane, 33 wt % liquid paraffin	0.7912	4.82	23.39

straight channel and the gas phase into the intersecting channel, forming the cross-flow rupturing process. For Group (B) of T-junction microfluidic devices, the liquid phase was pumped into the intersecting channel and the gas phase into the straight channel, forming the perpendicular rupturing process. For Group (C) symmetrically cross-shaped microfluidic devices, the liquid phase was pumped into the intersecting channel and the gas phase into the straight channel, forming the symmetrically perpendicular rupturing process.

Materials

Air at 25°C was used as the gas phase. Three different organic liquids (dodecane, hexadecane, and liquid paraffin) were used, either alone or by combining two different liquids, as the liquid phase. Four unique liquid–gas systems were used in the experiments, whose physical properties including density, viscosity and surface tension are listed in Table 1. The viscosities of the liquids were measured with an Ubbelohde viscometer at 25°C. The surface tension was measured with the pendant drop technique using a DataPhysics Instruments GmbH (Filderstadt). Dodecane and hexadecane were analytically pure and purchased from Sinopharm Chemical Reagent (China). Liquid paraffin was chemically pure and purchased from Beijing Chemical Plant.

Apparatus and analysis

Experiments were carried out with a microscope at 40× magnification. A high-speed CCD video camera was connected to the microscope, and images were recorded at a frequency of 200 images per second. The lengths of the slugs were measured from the microscope images, and after changing any of the flow parameters, 100 s of equilibration time was allowed.

Results and Discussion

Microbubbles formation in T-junction microfluidic devices with cross-flow rupturing

In our previous study, a modified T-junction microfluidic device was developed to form uniform gas-slug-in-water flow. The narrower channel at the intersection provides higher velocity in the dispersion process, whereas the wider main channel provides low pressure drop in the flowing process, both of them can help to stabilize the pressure of the gas phase during dispersion. In this part of experiment, this modification is adopted. The liquid phase was pumped into the straight channel and the gas phase into the intersecting channel, forming the cross-flow rupturing process.

Flow patterns

Different two-phase flow patterns could be observed in the narrow channel, when the experimental conditions were varied. As shown in Figure 3, the flow patterns could be defined as Type 1, 2, and 3.

Type 1: Nonuniform slug flow appears at low liquid flow rate and viscosity. In this type of flow pattern, the shear force of the liquid is not enough for squeezing the gas phase. Liquid single-phase flow and long-gas-slug-in-liquid flow, respectively, appear periodically.

Type 2: Uniform dispersed slug flow appears when the flow rate and viscosity of the liquid phase increase and at proper gas flow rate. In this type of flow pattern, the uniform slugs are formed in the narrow channel, forming uniform isolate bubbles flow in the main channel. The polydispersity index (σ) value is less than 5% in this flow pattern type. σ is defined by $\sigma = \delta/d_{av}$, in which δ is the standard deviation and d_{av} is the average bubble diameter.

Type 3: In this type of flow pattern, uniform slug or bubble flow appears at the main channel, not at the narrow channel. There are two possibilities for this type of flow pattern. When the gas flow rate increases based on Type 2, the formed slugs are too long to be dispersed in the narrow channel and are dispersed by the effect of expansion in the main channel. As the viscosity and flow rate of the liquid phase increase, breakup does not occur in the narrow channel, but phenomenon similar to the two-phase laminar flow appears. The "laminar flow" breakup by the effect of expansion and multiple-bubble layer as well as zig–zag patterns appears in the main channel.

The flow regime transition for different dispersion methods will be discussed in the last section. The dispersion mechanism of Type 2 flow pattern is discussed in this section.

Mechanism study

Several parameters were investigated to determine their influences on slug length. As shown in Figures 4a, b, the

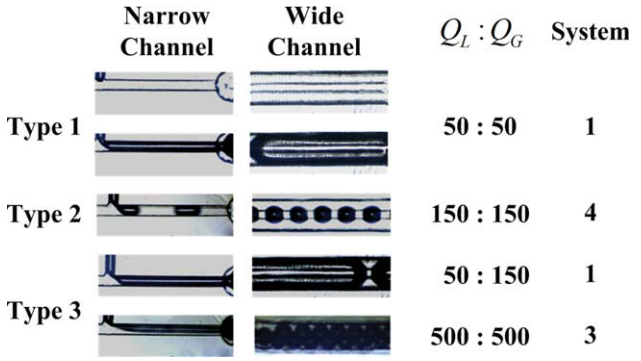

Figure 3. Two-phase flow patterns at different systems and flow rates.

[Color figure can be viewed in the online issue, which is available at wileyonlinelibrary.com.]

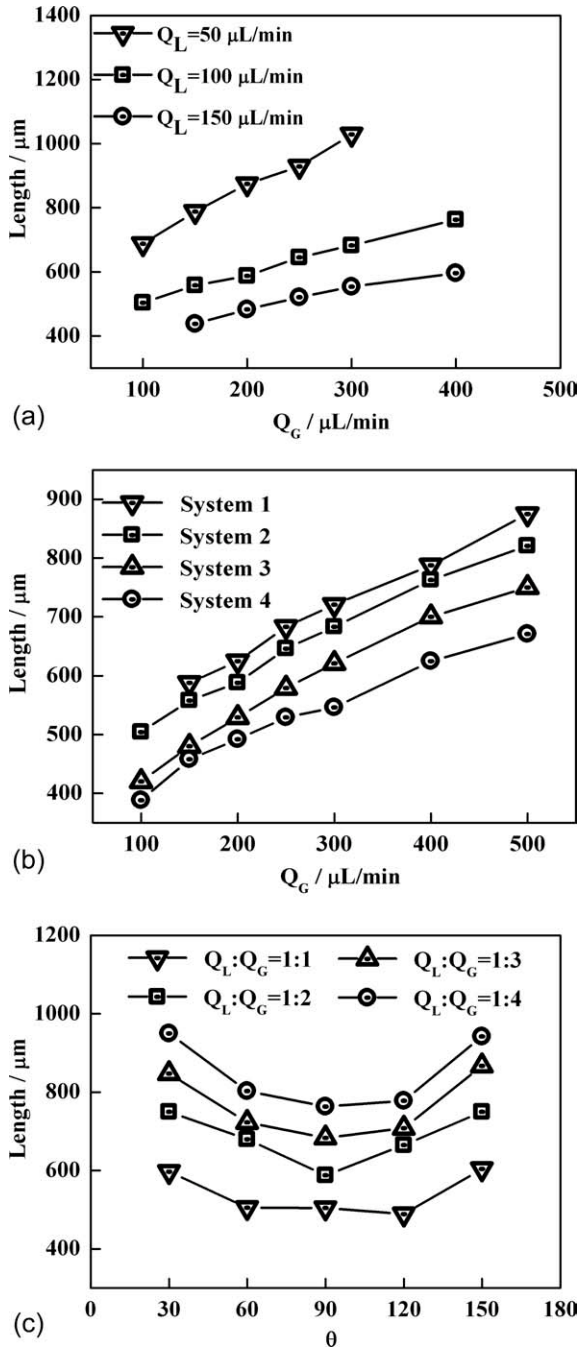

Figure 4. Influences of parameters on slug length with cross-flowing shear rupturing.

(a) Influences of two-phase flow rates, liquid phase: System 2, $\theta = 90°$; (b) influences of viscosity of liquid phase, $Q_L = 100$ μL/min, $\theta = 90°$; and (c) influences of Q_G/Q_L and intersection angle θ, $Q_L = 100$ μL/min, liquid phase: System 2.

slug length decreases with the increase in the velocity and viscosity of the liquid phase. The change of slug length may be caused by the influence of the shear force of the liquid phase. As shown in Figure 4c, the slug length increases with the increase of the two-phase flow ratio Q_G/Q_L, in which Q_G is the flow rate of the gas phase and Q_L is the flow rate of the liquid phase. It is worth noting that the slug length is influenced by the microchannel intersection angle θ. As shown in Figure 4c, the slug length reaches a minimum value when $\theta = 90°$ and increases when θ changes away from 90°. Figure 5 shows the interfacial shapes both at the beginning and at the end of the breakup process for different microchannel intersection angles. When $\theta = 90°$, the breakup process produces plugs with the shortest neck length, and the neck length becomes longer as θ moves away from 90°. This may caused by the lower efficiency of the liquid phase to displace gas phase and occupy the cross section as well as the concurrent ($\theta < 90°$) or countercurrent ($\theta > 90°$) progress of two phases in the parallel direction. The difference of the transformation of the interface shape may be a main factor in the difference of dispersion size.

Recent studies[32–37] on liquid–liquid coflowing systems have shown that slug flow is observed at very low continuous-phase flow rates, followed by dripping and eventually tip streaming as the flow rate increases. Another study[38] has also shown that the production of gas–liquid and liquid–liquid two-phase slug flow in T-junction microfluidic devices is governed by two different mechanisms: squeezing and shearing. The squeezing mechanism exerts dominant control over droplet breakup at low Ca numbers, defined as $Ca = u_c\mu/\gamma$, where u_c is the flow rate of continuous phase, μ is the viscosity of continuous phase, and γ is interfacial tension of two phases, whereas the shearing mechanism is dominant at high Ca numbers. In the squeezing regime at low Ca numbers, interfacial force is dominant and the emerging bubble or droplet fills most of the channel while the continuous phase pushes the dispersed phase forward until it snaps off. At higher Ca numbers in the shearing regime, the shearing force is dominant and the bubble or droplet is sheared off by the continuous phase before it occupies the cross section of the channel. The transition from squeezing regime to dripping regime for liquid–liquid two-phase flow in T-junction microchannels occurred at the value of Ca number on the order of 10^{-2} with 200-μm channel width[39] and around $Ca = 3 \times 10^{-3}$ with 100-μm channel width.[40] The transition for gas–liquid two-phase flow is reported to be $Ca = 5.8 \times 10^{-3}$.[41] In our experiments, the maximum of Ca number is 0.012, and only squeezing regime is obtained. Similar variation of the dispersed size is reported in the literature.[42–44]

The dispersion process could be considered to be affected by two major factors: the breakup rate and the transformation of the interface shape. The breakup process could be considered as the process at the balance between shear force and

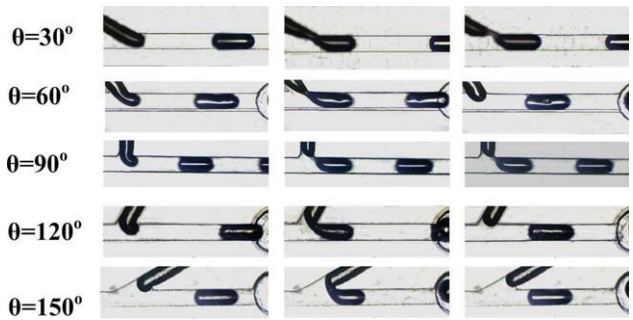

Figure 5. Images of gas rupture events with different intersection angles.

Liquid phase: System 4, $Q_G = 50$ μL/min, $Q_L = 50$ μL/min. [Color figure can be viewed in the online issue, which is available at wileyonlinelibrary.com.]

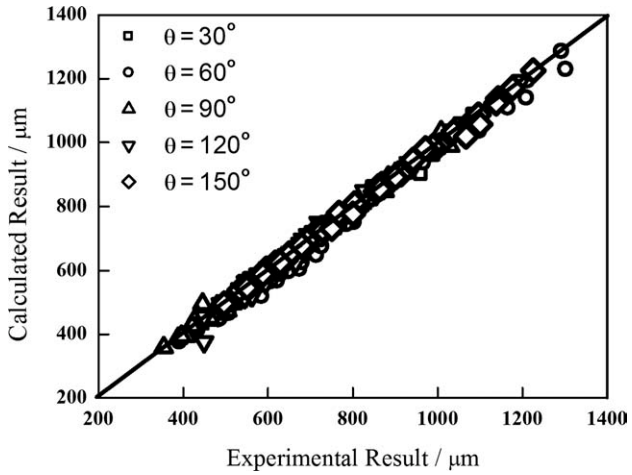

Figure 6. Comparison between calculated results and experimental data.

interfacial force. Therefore, the breakup rate could be characterized by the capillary number, Ca, which is verified by numerical study.[45] The transformation of the interface shape could be characterized by the two-phase flow ratio Q_G/Q_L when intersection angle $\theta = 90°$. Considering both the factors, the slug length can be expressed as

$$L/w = k\left(\frac{Q_G}{Q_L}\right)^{\alpha} \mathrm{Ca}^{\beta} \tag{1}$$

in which L is the slug length, w is the width of the channel, k, α, and β are the parameters related to the device structure and dispersion method.

When intersection angle θ differs from 90°, expression can also describe the dispersion process as some modification made on the factors. As described above, θ influences the effective component of the liquid shearing force acting on the gas phase. As θ changes away from 90°, the effective component decreases. Thus, the effective component may be modified to $Q_L \sin\theta$. Therefore, Q_G/Q_L can be modified to be $\frac{Q_G}{Q_L \sin\theta}$.

The shear force affects at the head of the gas phase, which is in the straight channel. The intersection angle θ does not impact the liquid velocity in the main channel. Thus, there is no need to modify the capillary number Ca when intersection angle θ changes.

A linear regression was used to evaluate the parameters from data in Figure 4, showing that $k = 0.75$, $\alpha = 0.33$, and $\beta = -0.20$. The slug length formed in the T-junction microfluidic device with cross-flowing rupturing can be predicted by Eq. 2.

$$L/w = 0.75\left(\frac{Q_G}{Q_L \sin\theta}\right)^{0.33} Ca^{-0.20} \tag{2}$$

As shown in Figure 6, Eq. 2 provides good prediction for Type 2 pattern.

Microbubbles formation in T-junction microfluidic devices with perpendicular rupturing

In this part of experiments, the liquid phase was pumped into the intersecting channel and the gas phase into the straight channel, forming perpendicular rupturing process. Similar to cross-flow rupturing, flow patterns Type 1, 2, and 3 as described in the section of cross-flow rupturing could be observed in the narrow channel. The flow regime transition for different dispersion methods will be also discussed in the last section, and mechanism of Type 2 pattern is discussed in this section.

Similar parameters to cross-flow rupturing were investigated to determine their influences on the slug length. The

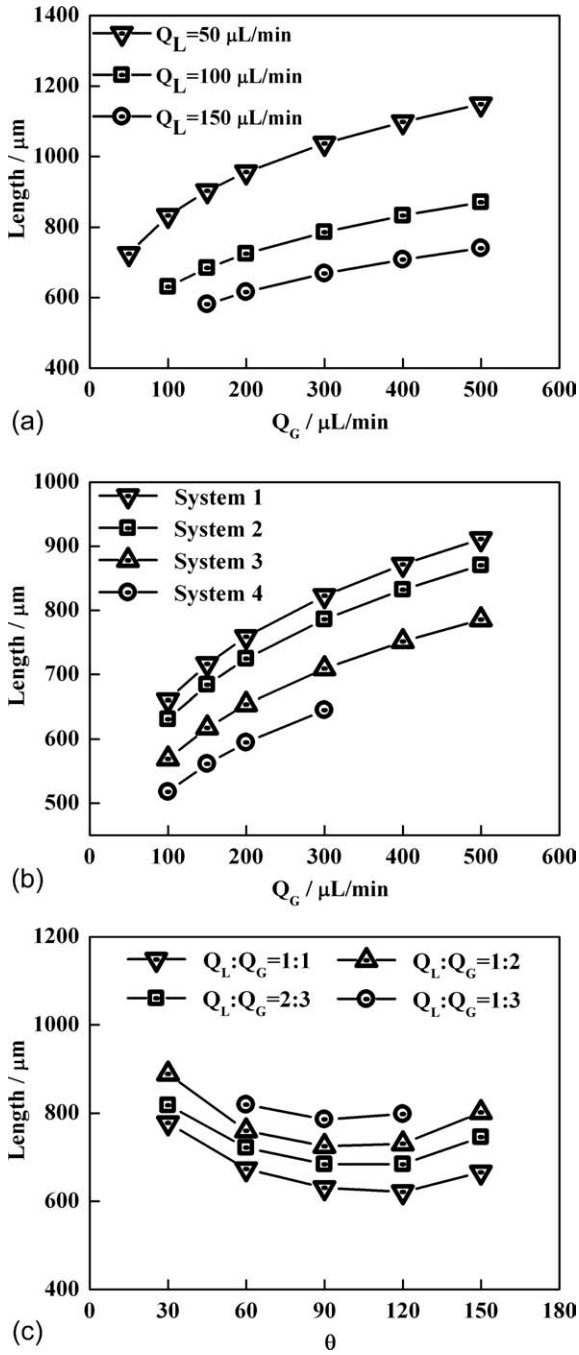

Figure 7. Influences of parameters on slug length with perpendicular rupturing.

(a) Influences of two-phase flow rates, liquid phase: System 2, $\theta = 90°$; (b) influences of viscosity of liquid phase, $Q_L = 100$ μL/min, $\theta = 90°$; and (c) influences of Q_G/Q_L and intersection angle θ, $Q_L = 100$ μL/min, liquid phase: System 2.

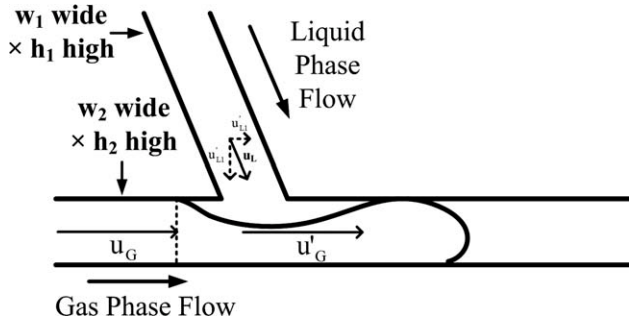

Figure 8. Sketch of the rupture process at the intersection of perpendicular rupturing.

slug length decreases with the increase in the velocity (Figure 7a) and viscosity (Figure 7b) of the liquid phase. As shown in Figure 7c, the slug length increases with the increase of the two-phase flow ratio Q_G/Q_L, and the slug length reaches a minimum value when $\theta = 90°$. The results are similar to those with the method of cross-flow rupturing. Also, they are similar to those in the same devices for gas/water systems.[29]

As mentioned above, transformation of interfacial shape and balance between shear force and interfacial tension are considered to be two major factors affecting dispersion process in squeezing regime. Thus, the slug length can be expressed as $L/w = k(Q_G/Q_L)^{\alpha}Ca^{\beta}$, in which a modification of two-phase flow ratio Q_G/Q_L and capillary number Ca should be considered when intersection angle is θ.

Similar to the cross-flow rupturing process, the capillary number Ca is not influenced by the intersection angle θ, and no modification is required when intersection angle θ changes.

The modification of flow ratio Q_G/Q_L in the perpendicular rupturing process should consider both the influence of the perpendicular component of the liquid velocity on rupturing velocity and horizontal component of the liquid velocity on the gas-phase flow. The schematic diagram is shown as Figure 8, and the details of modification are described in our previous work.[29] After modification, Q_G/Q_L is expressed as

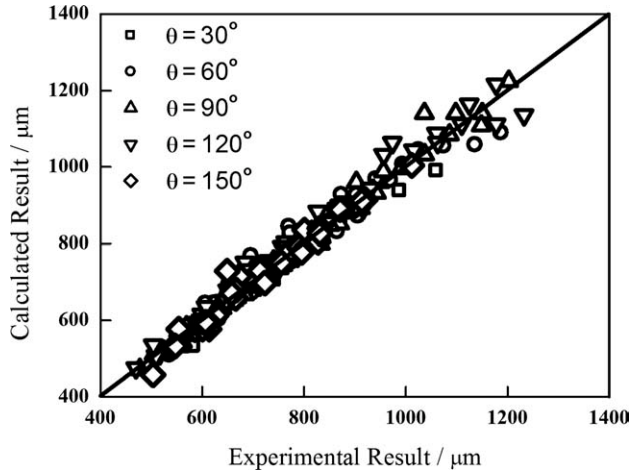

Figure 9. Comparison between calculated results and experimental data with perpendicular rupturing.

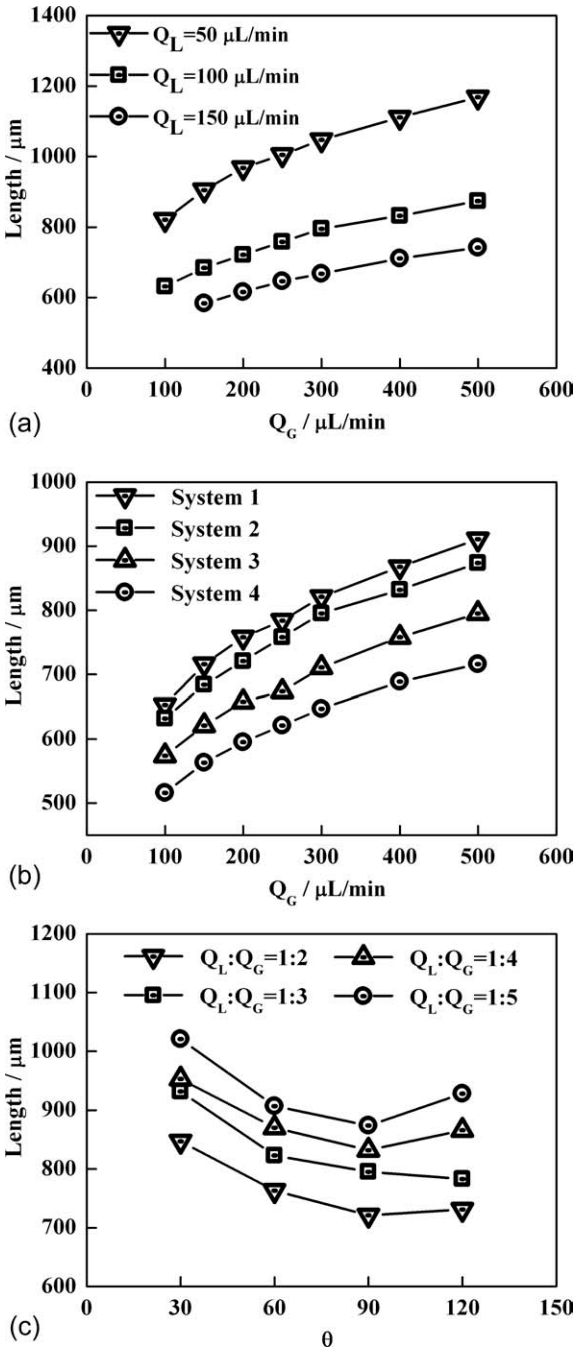

Figure 10. Influences of parameters on slug length with symmetrically perpendicular rupturing.

(a) Influences of two-phase flow rates, liquid phase: System 2, $\theta = 90°$; (b) influences of viscosity of liquid phase, $Q_L = 100$ μL/min, $\theta = 90°$; and (c) influences of Q_G/Q_L and intersection angle θ, $Q_L = 100$ μL/min, liquid phase: System 2.

$\frac{Q_G}{Q_L \sin\theta} + \lambda \cot\theta$, in which λ is an efficiency coefficient equal to λ_1 when $\theta < 90°$ and λ_2 when $\theta > 90°$.

A linear regression was used to evaluate the parameters from data in Figure 7, showing that $k = 1$, $\lambda_1 = \lambda_2 = 0.40$, $\alpha = 0.20$, and $\beta = -0.20$.

The slug length formed in a T-junction microfluidic device with perpendicular rupturing can be predicted by Eq. 3.

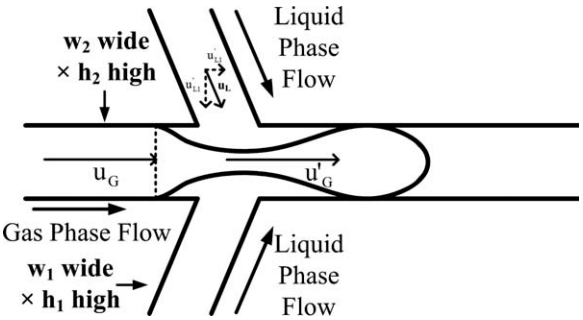

Figure 11. Sketch of the rupture process of slug at the intersection of symmetrically perpendicular rupturing.

$$L/w = \left(\frac{Q_G}{Q_L \sin\theta} + 0.40\cot\ \theta\right)^{0.20} Ca^{-0.20} \qquad (3)$$

As shown in Figure 9, Eq. 3 provides good prediction.

Microbubbles formation in symmetrical cross-shaped microfluidic devices with symmetrically perpendicular rupturing

In this section, the liquid phase was pumped into the symmetrical intersecting channels and the gas phase into the straight channel, forming a symmetrical perpendicular rupturing process. Q_L is the total liquid-phase flow rate, and, thus, the value for each intersecting channel is $\frac{1}{2}Q_L$.

Experiments were conducted similarly to those described above for cross flow and perpendicular rupturing in T-junction microfluidic devices, and the three different flow patterns (Type 1, 2, and 3) were produced by changing the liquid–gas flow rates, intersection angle, and liquid viscosity. The flow transitions for the three different dispersion methods as well as the breakup mechanism for the Type 2 flow pattern are discussed in this section.

Several parameters were investigated to determine their influences on slug length, showing similar varieties as asymmetrically perpendicular rupturing in T-junction microfluidic devices. Figure 10 shows that the relationships between slug length and flow velocity (a) and slug length and viscosity of the liquid phase (b) are similar to those seen for cross-flow and perpendicular rupturing. As shown in Figure 10c, the slug length increases with the increase of the two-phase flow ratio Q_G/Q_L, and slug length reaches a minimum value when $\theta = 90°$.

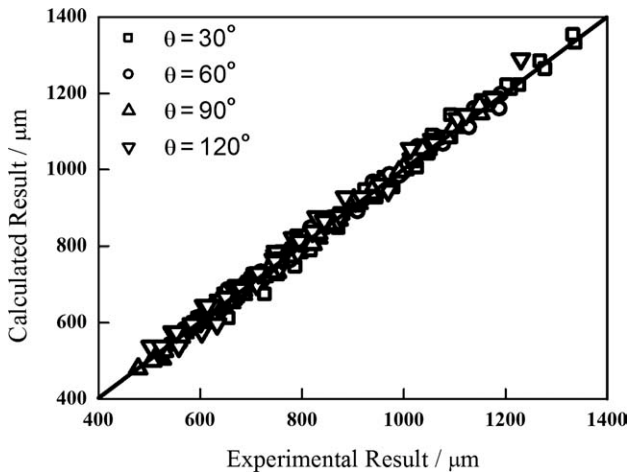

Figure 12. Comparison between calculated results and experimental data with symmetrically perpendicular rupturing.

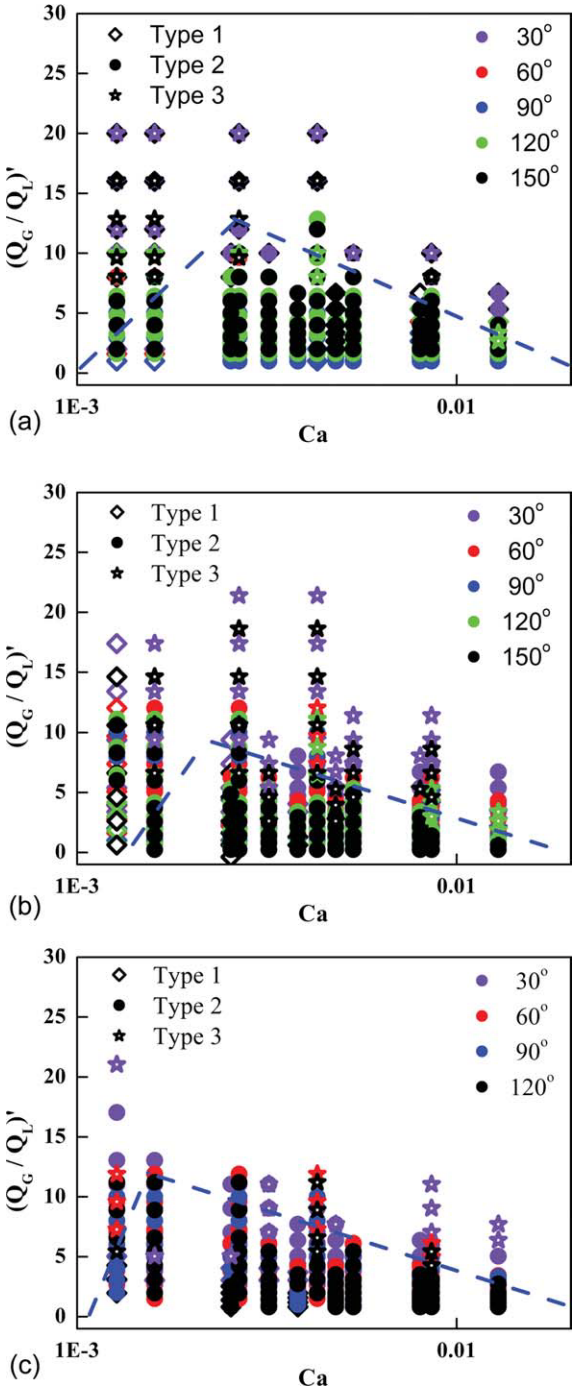

Figure 13. Flow regime transition.

(a) Cross-flow rupturing; (b) perpendicular rupturing; and (c)symmetrically perpendicular rupturing. [Color figure can be viewed in the online issue, which is available at wileyonlinelibrary.com.]

Table 2. Comparison of Dispersion Size with Different Dispersion Methods

$L/w = k(Q_G/Q_L)^{\alpha}Ca^{\beta}$	Cross-Flow Rupturing	Perpendicular Rupturing	Symmetrically Perpendicular Rupturing
$(Q_G/Q_L)'$	$\frac{Q_G}{Q_L \sin\theta}$	$\frac{Q_G}{Q_L \sin\theta} + \lambda \cot\theta$	$\frac{Q_G}{Q_L \sin\theta} + \lambda \cot\theta$
k	0.75	1	1
α	0.33	0.20	0.20
β	−0.20	−0.20	−0.20
λ	–	0.40	0.60

Here, the slug length is also expressed as $L/w = k(Q_G/Q_L)^{\alpha}Ca^{\beta}$. When intersection angle is θ, Q_G/Q_L is modified to $\frac{Q_G}{Q_L \sin\theta} + \lambda_3 \cot\theta$ and Ca number remains the same value as $\theta = 90°$, considering the comparability of asymmetrical and symmetrical perpendicular rupturing. The sketch diagram is shown in Figure 11.

A linear regression was used to evaluate the parameters from data in Figure 10, showing that $k = 1$, $\lambda_3 = 0.60$, $\alpha = 0.20$, and $\beta = -0.20$.

The slug length formed in the symmetrical cross microfluidic devices with perpendicular rupturing can be predicted as

$$L/w = \left(\frac{Q_G}{Q_L \sin\theta} + 0.60 \cot\theta\right)^{0.20} Ca^{-0.20} \quad (4)$$

As shown in Figure 12, Eq. 4 provides good prediction.

Comparison of microbubbles formation with different dispersion methods

Flow Regime Transition According to the discussion above, there are two major factors affecting the microdispersion process: the breakup rate and the transformation of the interface shape. They could also be considered as major factors causing flow regime transition in devices with different dispersion methods. As shown in Figure 13, flow pattern Type 2 is obtained in a triangular region, respectively, for three dispersion methods, in flow pattern map divided by factors of Ca and $(Q_G/Q_L)'$ (Expressions of $(Q_G/Q_L)'$ for different dispersion methods are listed in Table 2). In cross-flow rupturing mode, flow pattern of uniform slug flow dispersed in narrow channel appears within a wider range of conditions, which may be caused by the higher shearing efficiency of the liquid phase and stability of the gas phase.

Scaling of Slug Length. As discussed in the above three sections, the slug length in the T-junction and symmetrically

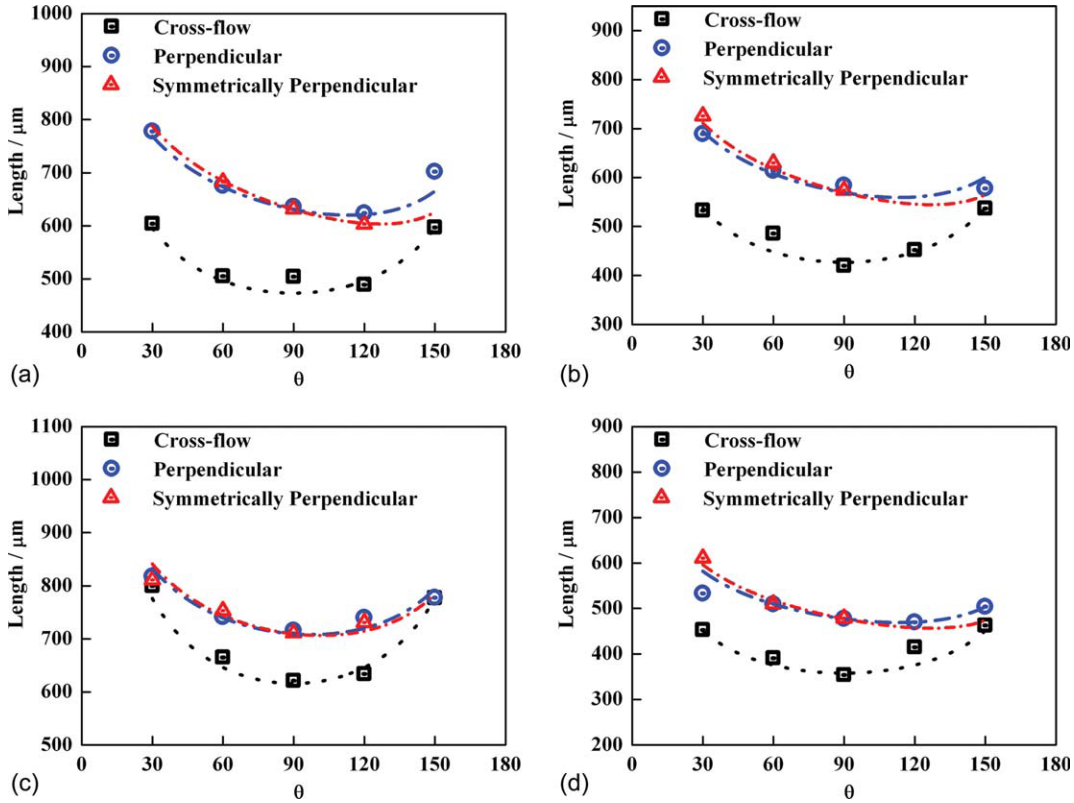

Figure 14. Comparison of dispersion size with different dispersion methods.

Symbols show experimental result, and lines show values calculated by prediction equations. (a) Liquid phase: System 2, $Q_G = 100$ μL/min, $Q_L = 100$ μL/min; (b) liquid phase: System 3, $Q_G = 100$ μL/min, $Q_L = 100$ μL/min; (c) liquid phase: System 3, $Q_G = 100$ μL/min, $Q_L = 300$ μL/min; and (d) liquid phase: System 4, $Q_G = 150$ μL/min, $Q_L = 150$ μL/min. [Color figure can be viewed in the online issue, which is available at wileyonlinelibrary.com.]

cross-shaped microfluidic devices with different dispersion methods can be expressed as $L/w = k(Q_G/Q_L)^{\alpha}Ca^{\beta}$, with different modification of $(Q_G/Q_L)'$ and empirical coefficients, respectively. Table 2 shows the comparison of modification of $(Q_G/Q_L)'$ and empirical coefficients with different dispersion methods. Figure 14 shows the comparison of calculated size of three dispersion methods with the same system and operation conditions. The cross-flow shearing mode provides smaller dispersion size, which is caused by a faster interface deformation progress—it is easier for the liquid phase to displace gas phase and occupy the cross section than for gas phase to displace liquid phase due to the inertia comparison of the two phases and, thus, liquid phase shows higher ''cut-off efficiency'' in the cross-flow shearing mode. The size difference among dispersion methods is greater when shear force of liquid phase is small (at low flow rate and viscosity of liquid phase). The intersection angle shows greater effect on the dispersion size in symmetrically perpendicular rupturing mode than in asymmetrically perpendicular rupturing mode, which is caused by the greater influence of the horizontal component of liquid velocity on gas-phase flow. The difference is greater when (Q_G/Q_L) is lower.

Conclusion

In this article, we developed organic solvent–gas dispersed flow without surfactant in T-junction and symmetrical cross-shaped microfluidic devices to understand the process of gas dispersing in organic solvents at microscale for its important and widely applications in gas–liquid reaction and separation processes. Three most commonly used dispersion methods were used, including cross-flow rupturing, perpendicular rupturing, and symmetrically perpendicular rupturing. Different flow patterns and dispersion size appear with the variation of two-phase flow rates, viscosity of liquid phase, and intersection angle, respectively, with each dispersion method. The results showed that there were three typical flow patterns in microchannels defined as Type 1, 2, and 3. In the flow pattern of Type 2, uniform gas slugs were formed in the narrow channel, forming uniform isolate bubbles flow in the main channel. Then, the systematic investigation and discussion of the scaling of gas slug formation in the flow pattern of Type 2 was carried out. Two major factors were considered to influence the dispersion process: the breakup rate and the transformation of the interface shape. A unified equation $L/w = k(Q_G/Q_L)^{\alpha}Ca^{\beta}$ was used to predict the dispersion size, in which (Q_G/Q_L) was modified to different forms, respectively, for different dispersion methods, considering the influence of intersection angle on the transformation of the interface shape. Three models were developed to predict the dispersion size, and the calculated data were in good agreement with the experimental results. Comparison of different dispersion methods shows that dispersion method of cross-flow rupturing helps to form smaller dispersion size with the same flow rate of liquid phase, which may caused by a faster interface deformation progress because of higher ''cut-off efficiency'' of the liquid phase. Investigation above can, thus, potentially be useful in achieving a precisely controlled preparation of monodisperse gas bubbles in organic solvents for the application of gas–liquid microdispersion technology.

Acknowledgments

The authors acknowledge the support of the National Natural Science Foundation of China (20876084 and 20806042) and SRFDP (20090002110070) for this work.

Literature Cited

1. Skyba DM, Kaul S. Advances in microbubble technology. *Coron Artery Dis*. 2000;11:211–219.
2. Grinstaff MW, Suslick KS. Air-filled proteinaceous microbubbles: synthesis of an echo-contrast agent. *Proc Natl Acad Sci USA*. 1991; 88:7708–7710.
3. Choung JW, Luttrell GH, Yoon RH. Characterization of operating parameters in the cleaning zone of microbubble column flotation. *Int J Miner Process*. 1993;39:31–40.
4. Li B, Tao D, Ou Z, Liu J. Cyclo-microbubble column flotation of fine coal. *Sep Sci Technol*. 2003;38:1125–1140.
5. Tegrotenhuis WE, Cameron RJ, Viswanathan VV, Wegeng RS. Solvent extraction and gas absorption using microchannel contactors. *Microreaction Technology: Industrial Prospects: 3rd International Conference on Microreaction Technology*. New Orleans, LA, 2000: 541–549.
6. Chambers RD, Holling D, Spink RCH, Sandford G. Gas–liquid thin film microreactors for selective direct fluorination. *Lab Chip*. 2001; 1:132–137.
7. Hessel V, Ehrfeld W, Golbig K, Haverkamp V, Löwe H, Storz M, Wille C, Guber A, Jähnisch K, Baerns M. Gas/liquid microreactors for direct fluorination of aromatic compounds using elemental fluorine. *Microreaction Technology: Industrial Prospects: 3rd International Conference on Microreaction Technology*. New Orleans, LA, 2000:526–540.
8. Jahnisch K, Baerns M, Hessel V, Ehrfeld W, Haverkamp W, Löwe H, Wille C, Guber A. Direct fluorination of toluene using elemental fluorine in gas/liquid microreactors. *J Fluorine Chem*. 2000;105:117–128.
9. de Mas N, Jackman RJ, Schmidt MA, Jensen KF. Microchemical systems for direct fluorination of aromatics. *Microreaction Technology: 5th International Conference on Microreaction Technology*. Strasbourg, France, 2001:60–67.
10. Antes J, Tuercke T, Marioth E, Lechner F, Scholz M, Schnürer F, Krause HH, Löbbecke S. Investigation, analysis and optimization of exothermic nitrations in microreactor processes. *Microreaction Technology: 5th International Conference on Microreaction Technology*. Strasbourg, France, 2001:446–454.
11. Inoue T, Schmidt MA, Jensen KF. Microfabricated multiphase reactors for the direct synthesis of hydrogen peroxide from hydrogen and oxygen. *Ind Eng Chem Res*. 2007;46:1153–1160.
12. Burns MA, Mastrangelo CH, Sammarco TS, Man FP, Webster JR, Johnson BR, Foerster B, Jones D, Fields Y, Kaiser AR, Burke DT. Microfabricated structures for integrated DNA analysis. *Proc Natl Acad Sci USA*. 1996;93:5556–5561.
13. Garstecki P, Fischbach MA, Whitesides GM. Design for mixing using bubbles in branched microfluidic channels. *Appl Phys Lett*. 2005;86:244108.
14. Gunther A, Khan SA, Thalmann M, Trachsel F, Jensen KF. Transport and reaction in microscale segmented gas–liquid flow. *Lab Chip*. 2004;4:278–286.
15. Fu AY, Spence C, Scherer A, Arnold FH, Quake SR. A microfabricated fluorescence-activated cell sorter. *Nat Biotechnol*. 1999;17: 1109–1111.
16. Ramsey JD, Jacobson SC, Culbertson CT, Ramsey JM. High-efficiency, two-dimensional separations of protein digests on microfluidic devices. *Anal Chem*. 2003;75:3758–3764.
17. Chen XX, Wu HK, Mao CD, Whitesides GM. A prototype two-dimensional capillary electrophoresis system fabricated in poly(dimethylsiloxane). *Anal Chem*. 2002;74:1772–1778.
18. Song H, Ismagilov RF. Millisecond kinetics on a microfluidic chip using nanoliters of reagents. *J Am Chem Soc*. 2003;125:14613–14619.
19. Seong GH, Heo J, Crooks RM. Measurement of enzyme kinetics using a continuous-flow microfluidic system. *Anal Chem*. 2003;75:3161–3167.
20. Hansen CL, Skordalakes E, Berger JM, Quake SR. A robust and scalable microfluidic metering method that allows protein crystal growth by free interface diffusion. *Proc Natl Acad Sci USA*. 2002; 99:16531–16536.

21. Zheng B, Roach LS, Ismagilov RF. Screening of protein crystallization conditions on a microfluidic chip using nanoliter-size droplets. *J Am Chem Soc*. 2003;125:11170–11171.
22. Ganan-Calvo AM, Gordillo JM. Perfectly monodisperse microbubbling by capillary flow focusing. *Phys Rev Lett*. 2001;87:274501.
23. Ganan-Calvo AM. Perfectly monodisperse microbubbling by capillary flow focusing: an alternate physical description and universal scaling. *Phys Rev E*. 2004;69:027301.
24. Gordillo JM, Cheng ZD, Ganan-Calvo AM, Marquez M, Weitz DA. A new device for the generation of microbubbles. *Phys Fluids*. 2004;16:2828–2834.
25. Garstecki P, Gitlin I, Diluzio W, Kumacheva E, Stone HA, Whitesides GM. Formation of monodisperse bubbles in a microfluidic flow-focusing device. *Appl Phys Lett*. 2003;85:2649–2651
26. Garstecki P, Stone HA, Whitesides GM. Mechanism for flow-rate controlled breakup in confined geometries: a route to monodisperse emulsions. *Phys Rev Lett*. 2005;94:164501.
27. Yasuno M, Iwamoto M, Sugiura S, Nakajima SM, Shono A, Satoh K. Monodispersed microbubble formation using microchannel technique. *AIChE J*. 2004;50:3227–3233.
28. Xu JH, Li SW, Wang YJ, Luo GS. Controllable gas-liquid phase flow patterns and monodisperse microbubbles in a microfluidic T-junction device. *Appl Phys Lett*. 2006;88:133506.
29. Tan J, Li SW, Wang K, Luo GS. Gas–liquid flow in T-junction microfluidic devices with a new perpendicular rupturing flow route. *Chem Eng J*. 2009;146:428–433.
30. Kobayashi J, Mori Y, Okamoto K, Akiyama R, Ueno M, Kitamori T, Kobayashi S. A microfluidic device for conducting gas–liquid-solid hydrogenation reactions. *Science*. 2004;304:1305–1308.
31. Li SW, Wang YJ, Lu YC, Luo GS. Low-temperature bonding of poly-(methylmethacrylate) microfluidic devices under an ultrasonic field. *J Micromech Microeng*. 2009;19:015035.
32. Ganan-Calvo AM, Gonzalez-Prieto R, Riesco-Chueca P, Herrada MA, Flores-Mosquera M. Focusing capillary jets close to the continuum limit. *Nat Phys*. 2007;3:737–742.
33. Suryo R, Basaran OA. Tip streaming from a liquid drop forming from a tube in a co-flowing outer fluid. *Phys Fluids*. 2006;8:082102.
34. Basaran OA, Suryo R. The invisible jet. *Nat Phys*. 2007;3:679–680.
35. Christopher GF, Noharuddin NN, Taylor JA, Anna SL. Experimental observations of the squeezing-to-dripping transition in T-shaped microfluidic junctions. *Phys Rev E*. 2008;78:036317.
36. Lee W, Walker LM, Anna SL. Role of geometry and fluid properties in droplet and thread formation processes in planar flow focusing. *Phys Fluids*. 2009;21:032103.
37. Lee MH, Prasad V, Lee D. Microfluidic fabrication of stable nanoparticle-shelled bubbles. *Langmuir*. 2010;26:2227–2230.
38. van Steijn V, Kreutzer MT, Kleijn CR. μ-PIV study of the formation of segmented flow in microfluidic t-junctions. *Chem Eng Sci*. 2007;62:7505–7514.
39. Garstecki P, Fuerstman MJ, Stone HA, Whitesides GM. Formation of droplets and bubbles in a microfluidic T-junction—scaling and mechanism of break-up. *Lab Chip*. 2006;6:693–693.
40. Oishi M, Kinoshita H, Oshima M, Fujii T. Investigation of microdroplet formation in a T-shaped junction using multicolor confocal micro PIV. *1st ASME Micro/Nanoscale Heat Transfer International Conference*. Natl Cheng Kung Univ, Tainan, Taiwan, 2008:297–301.
41. Guo F, Chen B. Numerical study on Taylor bubble formation in a micro-channel T-junction using VOF method. *Microgravity Sci Technol*. 2009;21:51–58.
42. Xiong RQ, Chung JN. Bubble generation and transport in a microfluidic device with high aspect ratio. *Exp Ther Fluid Sci*. 2009;33:1156–1162.
43. Fries D, von Rohr PR. Impact of inlet design on mass transfer in gas-liquid rectangular microchannels. *Microfluid Nanofluid*. 2009;6:27–35.
44. Menetrier-Deremble L, Tabeling P. Droplet breakup in microfluidic junctions of arbitrary angles. *Phys Rev E*. 2006;74:035303.
45. Dai L, Cai WF, Xin F. Numerical study on bubble formation of a gas-liquid flow in a T-junction microchannel. *Chem Eng Technol*. 2009;32:1984–1991.

Manuscript received Aug. 9, 2010, and revision received Oct. 7, 2010.